J|A|C|S
ARTICLES
Published on Web 03/13/2007

Bimodal Bond-Length Distributions in Cobalt-Doped CdSe, ZnSe, and $Cd_{1-x}Zn_xSe$ Quantum Dots

Steven A. Santangelo, Eric A. Hinds, Vladimir A. Vlaskin, Paul I. Archer, and Daniel R. Gamelin*

Contribution from the Department of Chemistry, University of Washington, Seattle, Washington 98195-1700

Received November 17, 2006; E-mail: Gamelin@chem.washington.edu

Abstract: Electronic absorption spectroscopy has been used to study changes in Co^{2+} ligand-field parameters as a function of alloy composition in Co^{2+}-doped $Cd_{1-x}Zn_xSe$ nanocrystals. A shift in the energy of the $^4T_1(P)$ excited-state with alloy composition is observed. Analysis reveals that $Co^{2+}-Se^{2-}$ bond lengths change relatively little as the host is varied continuously from CdSe to ZnSe, generating a large difference between microscopic and average cation−anion bond lengths in Co^{2+}-doped CdSe nanocrystals but not in Co^{2+}-doped ZnSe nanocrystals. The bimodal bond-length distributions observed here are shown to cause a diameter-dependent enthalpic destabilization of doped semiconductor nanocrystals.

1. Introduction

X-ray diffraction (XRD) is commonly used as a probe of composition in crystalline alloys. According to Vegard's law, the lattice constants of an $A_{1-x}B_xE$ solid solution determined by XRD should vary linearly with composition (x). Extensive studies have demonstrated very close adherence to Vegard's law in bulk alloyed II−VI semiconductors.[1] Extended X-ray absorption fine structure (EXAFS) spectroscopic measurements on some of the same II−VI bulk alloys have revealed significant differences between average and microscopic cation−anion distances,[1−11] however, emphasizing that XRD is not sensitive to the microstructures of individual lattice points but instead reveals only structure parameters averaged over all lattice sites. Recently, Vegard's law has been applied to analyze II−VI $A_{1-x}B_xE$ semiconductor nanocrystals.[12−15] This traditional approach faces new complications when applied to alloyed nanocrystals because of the diameter-dependent XRD peak broadening, increased risk of phase segregation, and extremely high surface-to-volume ratios in nanocrystals.

In this study, we use Co^{2+} as a structural surrogate for Zn^{2+} to examine colloidal $Cd_{1-x}Zn_xSe$ nanocrystals in the range $0 < x < 1$. Tetrahedral Co^{2+} and Zn^{2+} are very similar: both are substantially smaller than Cd^{2+} (tetrahedral covalent radii:[4] Co^{2+}, 1.197; Zn^{2+}, 1.225; Cd^{2+}, 1.405 Å), the local Co^{2+} and Zn^{2+} cation−anion bond lengths in $Co^{2+}{}_{0.07}$:$Zn_{0.93}Se$ bulk crystals measured by EXAFS are nearly identical (2.433 ± 0.005 and 2.456 ± 0.005 Å, respectively),[5] and both ions have orbitally isotropic ground states to first order. In contrast with Zn^{2+} or Cd^{2+}, Co^{2+} has a partially unoccupied valence d shell and therefore exhibits sub-band gap electronic and magnetic transitions that are sensitive to its local coordination environment, as described by ligand-field theory. Because of this feature, Co^{2+} substitution has been widely used as a strategy for studying Zn^{2+} metalloenzyme active sites.[16] Recently, ligand-field transitions have also been used to monitor Co^{2+} speciation during the synthesis of doped semiconductor nanocrystals and, among other things, have allowed distinction between substitutional and surface-bound Co^{2+} ions on the basis of their different energies, intensities, bandshapes, and sensitivities to surface-capping ligation in these two scenarios.[17−19] Here, ligand-field absorption spectroscopy is used to probe the effects of alloy composition variation on microscopic bonding parameters. Analysis of the ligand-field transition energies of Co^{2+} ions in $Cd_{1-x}Zn_xSe$ nanocrystals reveals that the $Co^{2+}-Se^{2-}$ bond lengths change relatively little across the entire range of compositions $\sim 0 < x$

(1) Furdyna, J. K., Kossut, J., Vol. Eds. *Diluted Magnetic Semiconductors*. Vol. 25 in *Semiconductors and Semimetals*; Willardson, R. K., Beer, A. C., Eds.; Academic Press: New York, 1988.
(2) Boyce, J. B.; Mikkelsen, J. C. J. *J. Cryst. Growth* **1989**, *98*, 37−43.
(3) Balzarotti, A.; Czyzyk, M.; Kisiel, A.; Motta, N.; Podgòrny, M.; Zimnal-Starnawska, M. *Phys. Rev. B* **1984**, *30*, 2295−2298.
(4) Iwanowski, R. J.; Lawniczak-Jablonska, K.; Golacki, Z.; Traverse, A. *Chem. Phys. Lett.* **1998**, *283*, 313−318.
(5) Lawniczak-Jablonska, K.; Golacki, Z. *Acta Phys. Pol. A* **1994**, *86*, 727−735.
(6) Lawniczak-Jablonska, K.; Libera, J.; Iwanowski, R. J. *J. Alloys Compd.* **1999**, *286*, 89−92.
(7) Cai, Y.; Thorpe, M. F. *Phys. Rev. B* **1992**, *46*, 15879−15886.
(8) Pong, W.-F.; Mayanovic, R. A.; Bunker, B. A.; Furdyna, J. K.; Debska, U. *Phys. Rev. B* **1990**, *41*, 8440−8448.
(9) Motta, N.; Balzarotti, A.; Letardi, P.; Kisiel, A.; Czyzyk, M. T.; Zimnal-Starnawska, M.; Podogorny, M. *J. Cryst. Growth* **1985**, *72*, 205−209.
(10) Motta, N.; Balzarotti, A.; Letardi, P.; Kisiel, A.; Czyzyk, M. T.; Zimnal-Starnawska, M.; Podgorny, M. *Solid State Commun.* **1985**, *53*, 509−512.
(11) Robouch, B. V.; Kisiel, A.; Konior, J. *J. Alloys Compd.* **2002**, *339*, 1−17.
(12) Hanif, K. M.; Meulenberg, R. W.; Strouse, G. F. *J. Am. Chem. Soc.* **2002**, *124*, 11495−11502.
(13) Zhong, X.; Feng, Y.; Knoll, W.; Han, M. *J. Am. Chem. Soc.* **2003**, *125*, 13559−13563.
(14) Raola, O. E.; Strouse, G. F. *Nano Lett.* **2002**, *2*, 1443−1447.
(15) Sung, Y.-M.; Lee, Y.-J.; Park, K.-S. *J. Am. Chem. Soc.* **2006**, *128*, 9002−9003.
(16) For a review, see: Maret, W.; Vallee, B. L. *Methods Enzymol.* **1993**, *226*, 52−71.
(17) Bryan, J. D.; Gamelin, D. R. *Prog. Inorg. Chem.* **2005**, *54*, 47−126.
(18) Radovanovic, P. V.; Gamelin, D. R. *J. Am. Chem. Soc.* **2001**, *123*, 12207−12214.
(19) Schwartz, D. A.; Norberg, N. S.; Nguyen, Q. P.; Parker, J. M.; Gamelin, D. R. *J. Am. Chem. Soc.* **2003**, *125*, 13205−13218.

$< \sim 1$. These results demonstrate the existence of alternating bond lengths in doped and alloyed nanocrystals. Such microscopic bond-length variations are shown to destabilize doped nanocrystals enthalpically with excess enthalpies that increase as the nanocrystal diameter decreases.

2. Experimental Section

The synthesis of $Cd_{1-x}(Zn + Co)_xSe$ nanocrystals was adapted from the procedure described recently for preparation of Co^{2+}-doped ZnSe nanocrystals.[20] Zinc oxide (ZnO, 98%), cobalt acetate tetrahydrate $Co(OAc)_2 \cdot 4H_2O$, 98.0%, GFS), cadmium oxide (CdO, 99.5%, Strem), oleic acid (OA, $C_{18}H_{36}O_2$, 97%, Acros), 1-hexadecylamine (HDA, $C_{16}H_{35}N$, 90%, Acros), 1-octadecene (ODE, $C_{18}H_{36}$, 90%, Aldrich), tributylphosphine (TBP, $C_{12}H_{27}P$, 97%, Aldrich), and selenium (Se, 99.5+%, Aldrich) were purchased and used as received. In 16.0 g of ODE, a solution of 0.2−0.6 mmol of ZnO, CdO, and $Co(OAc)_2 \cdot 4H_2O$ at the desired stoichiometry, 0.6−1.2 mmol of OA, and 0−1.6 mmol of HDA was prepared and purged with N_2 at 120 °C for ~1 h. A solution of ~2.4 mmol of Se and 4 mmol of TBP in 1.2 g of ODE was prepared in a glovebox and stored under N_2. The cation solution was heated to 310 °C, and the Se solution was rapidly injected using a gastight syringe. Following an initial drop in temperature after injection, the reaction solution was stabilized at 270−300 °C, where it was kept for several hours until alloying had completed. The reaction solution was then cooled, and the nanocrystals precipitated with a mixture of acetone and ethanol, were centrifuged, and were resuspended in toluene. The process of precipitation with ethanol and resuspension in toluene was repeated at least five times to remove excess reactants. These washed nanocrystals could be redispersed in nonpolar organic solvents. The synthesis is highly sensitive to starting conditions and produces a poor size distribution of particles, leaving substantial room for optimization.

Absorption spectra (298 K) of colloidal $Cd_{1-x}(Zn + Co)_xSe$ nanocrystals were collected using 1 cm cuvettes and a Cary 500 (Varian) spectrophotometer. Powder X-ray diffraction data were collected using a Rigaku Rotaflex RTP300 X-ray diffractometer. TEM images were obtained using a JEOL 2010F transmission electron microscope. The Co^{2+}, Zn^{2+}, and Cd^{2+} concentrations were determined quantitatively using an inductively coupled plasma atomic emission spectrometer (ICP-AES, Jarrel Ash model 955) after acid digestion of the samples.

3. Results and Analysis

3.1. Structure and Composition. Figure 1 summarizes (a) electronic absorption, (b) powder XRD, and (c−e) overview transmission electron microscopy (TEM) data for a series of ZnSe, $Cd_{1-x}Zn_xSe$, and CdSe nanocrystals, all pseudo-spherical with ~5 nm average diameters. The XRD data reveal that the CdSe and $Cd_{1-x}Zn_xSe$ nanocrystals adopt the wurtzite (w) lattice structure, whereas the ZnSe nanocrystals have the zinc blende (zb) structure. As anticipated, the band gap energy (E_g) of the $Cd_{1-x}Zn_xSe$ nanocrystals is between those of the CdSe and ZnSe nanocrystals. The average ZnSe and CdSe nanocrystal diameters ($d \approx 4.8$ and 4.6 nm, respectively) estimated from these absorption spectra using literature[21,22] relationships between diameter and E_g are consistent with those estimated from TEM ($d \approx 5.0$ and 4.8 nm, respectively).

In bulk $Cd_{1-x}Zn_xSe$ alloys, the dependence of E_g on x is not linear but instead it varies as a second-order equation in x as described by eq 1, where $E^i_{g,\infty}$ is the bulk band gap for i = ZnSe, alloy, or CdSe and b is the bowing parameter (for $Cd_{1-x}Zn_xSe$, $b = 0.35$).[23]

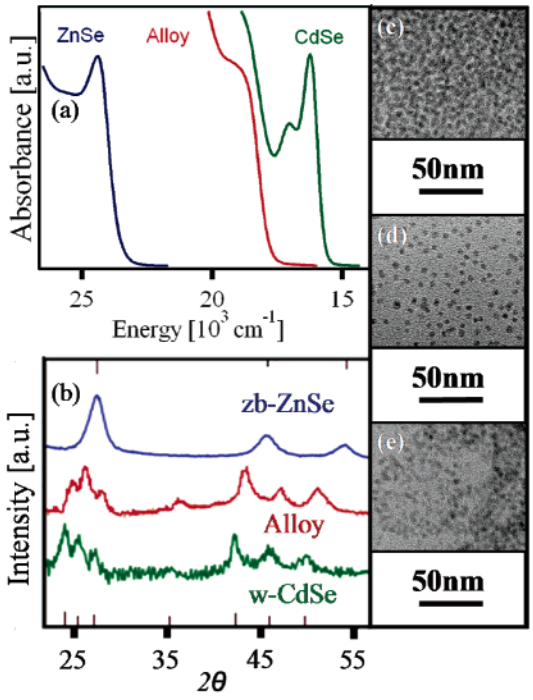

Figure 1. (a) 298 K electronic absorption spectra of colloidal CdSe (green), $Cd_{1-x}(Zn + Co)_xSe$ (red), and ZnSe (blue) nanocrystals. (b) Powder XRD data for CdSe (green), $Cd_{1-x}Zn_xSe$ (red), and ZnSe (blue) nanocrystals, with vertical marks showing the anticipated peak positions for w-CdSe and zb-ZnSe. Overview TEM images of (c) $d = 5.0$ nm ZnSe, (d) $d = 5.5$ nm $Cd_{1-x}Zn_xSe$, and (e) $d = 4.8$ nm CdSe nanocrystals.

$$E^{\text{alloy}}_{g,\infty}[x] = E^{\text{CdSe}}_{g,\infty}(1-x) + E^{\text{ZnSe}}_{g,\infty}(x) - bx(1-x) \quad (1)$$

In $Cd_{1-x}Zn_xSe$ nanocrystals, E_g also depends on the particle diameter (d). Modification of eq 1 to account for quantum confinement is therefore necessary. To describe the size dependence of E_g in quantum confined alloy nanocrystals, eq 1 is recast as a function of both d and x, as shown in eq 2.

$$E^{\text{alloy}}_{g}[d, x] = E^{\text{CdSe}}_{g,d}(1-x) + E^{\text{ZnSe}}_{g,d}(x) - bx(1-x) \quad (2)$$

From ref 22, the size dependence of E_g for ZnSe is given in the form of a power law expression. The literature expression is rewritten in eq 3 for clarity.

$$E^{\text{ZnSe}}_{g}[d] = E^{\text{ZnSe}}_{g,\infty} + \frac{2.08}{d^{1.19}} \quad (3)$$

The relationship between E_g and d in CdSe nanocrystals has been described previously using eq 4,[21] where λ(nm) refers to the wavelength of the first excitonic peak in the absorption spectrum.

$$d = (1.6122 \times 10^{-9})\lambda^4 - (2.6575 \times 10^{-6})\lambda^3 + (1.6242 \times 10^{-3})\lambda^2 - (0.4277)\lambda + 41.57 \quad (4)$$

Equation 4 can be rewritten in a form similar to that of eq 3 as shown in eq 5, where m and C are floating variables.

(20) Norberg, N. S.; Parks, G. L.; Salley, G. M.; Gamelin, D. R. *J. Am. Chem. Soc.* **2006**, *128*, 13195−13203.
(21) Yu, W. W.; Qu, L.; Guo, W.; Peng, X. *Chem. Mater.* **2003**, *15*, 2854−2860.
(22) Smith, C. A.; Lee, H. W. H.; Leppert, V. J.; Risbud, S. H. *Appl. Phys. Lett.* **1999**, *75*, 1688−1690.
(23) Poon, H. C.; Feng, Z. C.; Feng, Y. P.; Li, M. F. *J. Phys.: Condens. Matter* **1995**, *7*, 2783−2799.

$$E_g^{CdSe}[d] = E_{g,\infty}^{CdSe} + \frac{C}{d^m} \quad (5)$$

Fitting the experimental CdSe data of ref 21 with eq 5 yields $C = 1.83$ and $m = 1.06$. Substitution of eqs 3 and 5 into eq 2 then yields eq 6, which can now be used to describe band gap energy variations with alloy composition or particle diameter in quantum confined $Cd_{1-x}Zn_xSe$ nanocrystals.

$$E_g^{alloy}[d, x] = \left(E_{g,\infty}^{CdSe} + \frac{1.83}{d^{1.06}}\right)(1-x) + \left(E_{g,\infty}^{ZnSe} + \frac{2.08}{d^{1.19}}\right)x - bx(1-x) \quad (6)$$

To test eq 6, it can be used to estimate the composition of the alloy nanocrystals shown in Figure 1. Assuming b is independent of d, a value of $x = 0.37$ is estimated from the TEM diameters and the $Cd_{1-x}Zn_xSe$ absorption spectrum in Figure 1a using eq 6. Direct determination of the Cd:Zn ratio by inductively coupled plasma atomic emission spectrometry (ICP-AES) yields $x = 0.38$, and a value of $x = 0.38$ is also estimated from the XRD data in Figure 1b using Vegard's law. The excellent agreement among these three independent methods for evaluation of the alloy composition provides strong evidence in support of a random cation distribution in these $Cd_{1-x}Zn_xSe$ nanocrystals.

3.2. Ligand-Field Analysis. Figure 2 shows the Co^{2+} $^4A_2 \rightarrow {}^4T_1(P)$ ligand-field bands observed at 298 K in colloidal $Co^{2+}_{0.01}$:$Zn_{0.99}Se$, $Cd_{0.49}Zn_{0.42}Co_{0.09}Se$, and $Co^{2+}_{0.02}$:$Cd_{0.98}Se$ nanocrystals prepared by substituting the desired fraction of Zn^{2+} precursor with Co^{2+}. In each case, the degeneracy of the Co^{2+} $^4T_1(P)$ excited state is broken by the spin−orbit interaction, giving rise to the majority of the structure seen in these spectra. Comparison with absorption spectra of the corresponding Co^{2+}-doped ZnSe and CdSe bulk materials[24,25] verifies successful substitutional Co^{2+} incorporation into the ZnSe and CdSe nanocrystals. The $Cd_{0.49}Zn_{0.42}Co_{0.09}Se$ data in Figure 2 show no superposition of ligand-field bands at different energies as would arise from coexistence of distinct CdSe and ZnSe microenvironments but instead show a single ligand-field band with the same band shape but an intermediate energy. The observation that the peak width does not change with alloy composition provides further evidence of random cation distribution in the alloy nanocrystals. The continuous increase in the $^4T_1(P)$ energy with x (see Supporting Information) suggests that ligand-field electronic absorption spectroscopy might be useful as a spectroscopic analogue of XRD for composition determination in these and related alloy nanocrystals.

Ligand-field theory provides a clear understanding of the $^4A_2 \rightarrow {}^4T_1(P)$ transition energies in Figure 2. Figure 3 depicts the d^7 energy level diagram calculated for tetrahedral Co^{2+} ions by diagonalization of the appropriate Tanabe−Sugano energy matrices.[26] The results are plotted as the reduced energies of the various Co^{2+} terms above the $^4A_2$ ground state (E/B) vs the reduced ligand-field strength (Dq/B). The ligand-field parameters Dq and B are known for Co^{2+} in both CdSe and ZnSe bulk crystals and are provided in Table 1. To determine ligand-field parameters for Co^{2+} ions in the alloy nanocrystals, the "law"

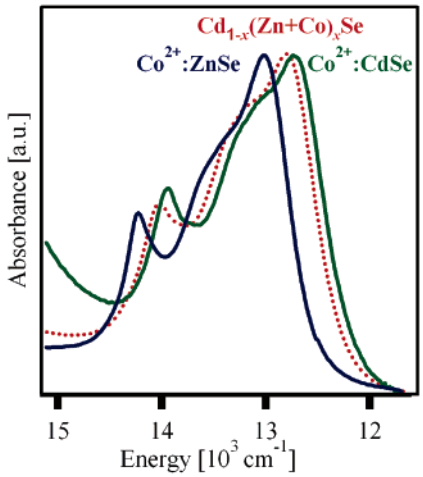

Figure 2. (a) Co^{2+} $^4A_2(F) \rightarrow {}^4T_1(P)$ absorption spectra in colloidal $Co^{2+}_{0.02}$:$Cd_{0.98}Se$ (green), $Cd_{0.49}Zn_{0.42}Co_{0.09}Se$ (red), and $Co^{2+}_{0.02}$:$Zn_{0.98}Se$ (blue) nanocrystals.

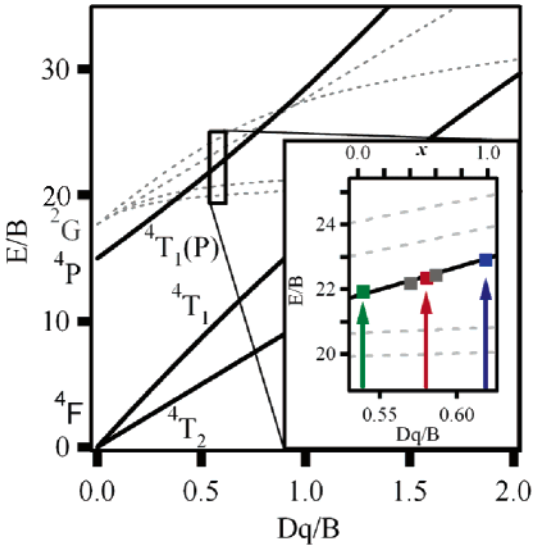

Figure 3. Tanabe−Sugano diagram calculated for Co^{2+} in a tetrahedral field ($B_{avg} = 591$ cm^{-1}, $C/B = 4.57$). Solid lines show quartet terms, and dashed lines show doublet terms. Inset: Expansion of the region probed experimentally with points plotting $E_{max}(^4A_2 \rightarrow {}^4T_1(P))$ from Figure 2.

of average environments was applied, which states that the effective Dq in a mixed ligand environment is approximately equal to the weighted average of the Dq values in each separate ligand set (eq 7). Extension to the electron−electron repulsion parameter (Racah B) is given in eq 8. This approach thus assumes that B and Dq vary linearly with x over the relatively small ranges sampled in the Co^{2+}-doped $Cd_{1-x}Zn_xSe$ alloy series (Table 1).

$$Dq[x] \approx Dq_{CdSe}(1-x) + Dq_{ZnSe}x \quad (7)$$

$$B[x] \approx B_{CdSe}(1-x) + B_{ZnSe}x \quad (8)$$

The inset of Figure 3 compares the relevant portion of the energy level diagram on an expanded scale with the experimental energies from Figure 2 and Table 1. Since the Racah parameters for Co^{2+} in CdSe and ZnSe are very similar ($B =$ 599 vs 584 cm^{-1}, respectively[27]), the $^4T_1(P)$ energies in Figure

(24) Tsai, T. Y.; Birnbaum, M. *J. Appl. Phys.* **2000**, *87*, 25−29.
(25) Langer, J. M.; Baranowski, J. M. *Phys. Status Solidi B* **1971**, *44*, 155−166.
(26) Tanabe, Y.; Sugano, S. *J. Phys. Soc. Jpn.* **1954**, *9*, 753−766.
(27) Dreyhsig, J.; Litzenburger, B. *Phys. Rev. B* **1996**, *54*, 10516−10524.

Table 1. Summary of Compositional, Ligand-Field Spectroscopic, and Microstructural Parameters for the $Cd_{1-x}(Zn + Co)_xSe$ Alloy Nanocrystals

	$Cd_{0.98}Co_{0.02}Se$ (2% Co^{2+}:CdSe)	$Cd_{0.61}Zn_{0.28}Co_{0.11}Se$	$Cd_{0.49}Zn_{0.42}Co_{0.09}Se$	$Cd_{0.41}Zn_{0.46}Co_{0.13}Se$	$Zn_{0.99}Co_{0.01}Se$ (1% Co^{2+}:ZnSe)
x	0.02	0.39	0.51	0.59	1.00
Co^{2+} $^4T_1(P)$ (E_{max}, cm^{-1})	12 720	12 734	12 800	12 898	13 201
Dq (cm^{-1})	322.6[27]	337.8	342.8	345.8	361.3[27]
B (cm^{-1})	598.5[27]	592.8	590.9	589.8	583.9[27]
a_{Co}[a] (Å)	2.484	2.466	2.459	2.454	2.433[5]
a_{avg} (Å)	2.63	2.56	2.54	2.52	2.45

[a] Mean value, from eq 10 and $n = 5.5$.

3 calculated using an average B (591 cm^{-1}) reproduce the experimental energies reasonably well across the entire range of compositions, justifying the use of eqs 7 and 8. The excellent overall agreement between calculated and experimental $^4T_1(P)$ variations with x shown in Figure 3 verifies the suitability of ligand-field theory for analysis of the spectra in Figure 2.

3.3. Co−Se Bond Lengths. From crystal-field theory, the parameter Dq depends microscopically upon the metal−ligand bond length (a) as described by eq 9, where Z_i is the effective nuclear charge of the transition metal ion, e is the charge of an electron, and $\overline{r^4}$ is the mean fourth power radius of the d electrons for the transition metal ion under consideration.[28] Empirically, $Dq \propto a^{-n}$ with $n = 5-6$.[28−31] From these relationships, eq 10 can be deduced and used to estimate the change in average $Co^{2+}-Se^{2-}$ bond length (a_{Co}) across the series of compositions in Figure 2.

$$Dq = \frac{Z_i e^2}{6a^5}\overline{r^4} \tag{9}$$

$$\frac{a}{a'} \approx \sqrt[n]{\frac{Dq'}{Dq}} \tag{10}$$

Using the values of Dq from Figure 3 and Table 1, eq 10 yields $a_{Co}(CdSe)/a_{Co}(ZnSe) \approx 1.023$ ($n = 5$)−1.019 ($n = 6$). Combining this result with the microscopic bond length $a_{Co}(ZnSe) = 2.433 \pm 0.005$ Å determined in $Co^{2+}_{0.07}$:$Zn_{0.93}Se$ bulk crystals by EXAFS analysis,[5] a_{Co} can be determined for the entire series of x from the data in Figure 3 and Table 1.

The bond lengths a_{Co} are plotted as a function of x in Figure 4 for $n = 5.5$ in eq 10. The dashed lines show that the results for $n = 5$ and 6 differ little because of the small overall change in Dq between the two endpoints. Figure 4 also compares a_{Co} with the average cation−anion bond lengths (a_{avg}) determined from XRD and Vegard's law. The striking conclusion derived from this analysis is that the increase in a_{Co} from $Co^{2+}_{0.01}$:$Zn_{0.99}Se$ ($a_{Co}(ZnSe) = 2.43$ Å) to $Co^{2+}_{0.02}$:$Cd_{0.98}Se$ ($a_{Co}(CdSe) \approx 2.48$ Å) is very small compared to the change in a_{avg} between the same two end points ($a_{Zn} = 2.45$ Å and $a_{Cd} = 2.63$ Å). The $Co^{2+}-Se^{2-}$ bonds elongate just ∼0.05 Å between $x \approx 1$ and $x \approx 0$ or only 28% as much as the elongation in a_{avg}. The $Co^{2+}-Se^{2-}$ bonds thus distort considerably less with x than would be inferred from XRD.

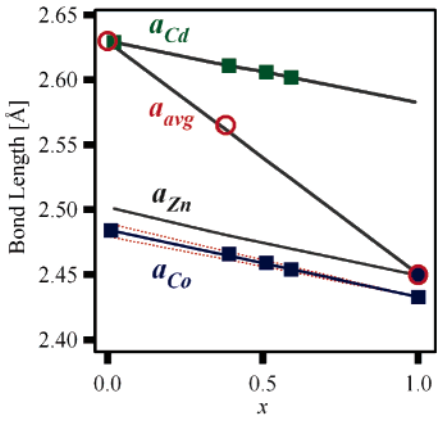

Figure 4. Cation−anion bond lengths as a function of composition, x, in $Cd_{1-x}(Zn + Co)_xSe$ alloy nanocrystals: $a_{Cd} = Cd^{2+}-Se^{2-}$ bond length. $a_{Zn} = Zn^{2+}-Se^{2-}$ bond length, a_{avg} = average cation−anion bond length from XRD and Vegard's law, and $a_{Co} = Co^{2+}-Se^{2-}$ bond length obtained using eq 10 and $n = 5.5$ (see text). The red broken lines depict the a_{Co} values obtained using $n = 5$ and 6.

Because Co^{2+} and Zn^{2+} have very similar bond lengths in $Co^{2+}_{0.07}$:$Zn_{0.93}Se$,[5] it is reasonable to infer a similar dependence on x for both a_{Co} and a_{Zn}. Additionally, because a_{avg} is the weighted average of the constituent bond lengths, a_{Cd} can also be estimated. The results of this analysis are summarized in Figure 4, which illustrates a bimodal bond-length distribution in which $a_{Co} \approx a_{Zn} < a_{Cd}$ for all x in $Cd_{1-x}(Zn + Co)_xSe$ nanocrystals.

These conclusions drawn for alloyed nanocrystals agree well with those drawn from systematic EXAFS analyses of related bulk ternary II−VI alloys.[1−8] For example, the increase of $Co^{2+}-Se^{2-}$ bond lengths by only 28% of the average cation−anion bond length increase in $Cd_{1-x}(Zn + Co)_xSe$ agrees well with the conclusion from bulk studies that cation−anion bond lengths typically change by only 20−25% of the average values across the full alloy range.[2] The value of $a_{Co}(CdSe) = 2.484$ Å estimated from the ligand-field analysis also compares reasonably well with the value of $a_{Co}(CdSe) = 2.43 \pm 0.01$ Å obtained from analysis of EXAFS data for $Co^{2+}_{0.04}$:$Cd_{0.96}Se$.[6] The discrepancy between $a_{Co}(CdSe)$ values determined by analysis of EXAFS and ligand-field absorption data (Figure 4) is substantially smaller than the differences between both and a_{Cd} in CdSe. Finally, the assertion that the conclusion drawn for Co^{2+} also applies to Zn^{2+} is supported by EXAFS results for $Cd_{1-x}Zn_xTe$ bulk alloys, which reveal $Zn^{2+}-Te^{2-}$ bond lengths that change only ∼20% as much as a_{avg} across the full alloy range ($a_{Zn-Te} = 2.670$ Å and $a_{Cd-Te} = 2.790$ Å in $Cd_{0.85}Zn_{0.15}Te$, vs $a_{Zn-Te} = 2.641$ Å in ZnTe and $a_{Cd-Te} = 2.802$

(28) Figgis, B. N.; Hitchman, M. A. *Ligand Field Theory and its Applications*; Wiley: New York, 2000, and references therein.
(29) Lever, A. B. P.; Walker, I. M.; McCarthy, P. J.; Mertes, K. B.; Jircitano, A.; Sheldon, R. *Inorg. Chem.* **1983**, *22*, 2252−2258.
(30) Hauser, A. *J. Chem. Phys.* **1991**, *94*, 2741−2748.
(31) Bray, K. L. *Top. Curr. Chem.* **2001**, *213*, 1−94.

Å in CdTe).[9−11] In general, therefore, the two spectroscopic approaches agree well.

3.4. Implications of Bimodal Bond-Length Distributions for Nanocrystal Doping. The observation of alternating bond lengths summarized in Figure 4 has important general implications for the synthesis of doped semiconductor nanocrystals. Impurity/host cation size mismatches have been suggested previously as important factors in nanocrystal doping by colloidal chemistry techniques.[17,18,32] In one example, Co^{2+} ions were found to be readily incorporated into ZnS nanocrystals during growth but under identical conditions were found to bind to CdS nanocrystal surfaces only after CdS growth slowed.[17,18] Since the ZnS and CdS nanocrystals prepared by this method are both cubic, their doping differences must arise from sources other than crystal morphology, a factor recently proposed to explain the different doping chemistries of wurtzite CdSe and cubic ZnSe nanocrystals by Mn^{2+}.[33] In the case of Co^{2+}:CdS, spectroscopic studies of surface-bound intermediates suggested that strong surface binding requires formation of a second $Co^{2+}-S^{2-}{}_{surface}$ bond and that formation of this bond can be very slow relative to CdS growth.[17,18]

Even after an impurity TM^{2+} ion binds strongly to a crystal surface, it still may not be readily incorporated into the internal volume of the growing nanocrystal because of increased crystal solubility in the locale of the impurity, i.e., lattice destabilization caused by the impurity. Inhibition of crystal growth by impurities has been widely documented,[34] including inhibition of II−VI semiconductor nanocrystal growth by isovalent impurities.[19] To quantify the lattice destabilization affected by such an impurity, the excess enthalpies of isovalent impurity mixing (ΔH_m) in ternary alloys have been investigated experimentally and theoretically.[35−37] In its simplest form, the excess enthalpy of mixing can be described using eq 11,[36,37] where the interaction parameter, Ω (kcal/mol), is proportional to the square of the difference between cation−anion bond lengths at the two endpoints AE and BE in the $A_{1-x}B_xE$ alloy composition range, i.e., $\Omega \propto (a_{AE} - a_{BE})^2$. Sizable bond-length differences such as those observed in Figure 4 can thus contribute substantial excess enthalpy disfavoring dopant incorporation into a growing crystallite. For illustration, the relative enthalpies of mixing for Co^{2+}:CdSe and Co^{2+}:ZnSe at a fixed value of x can be estimated from eq 11 as shown in eq 12.

$$\Delta H_m = x(1-x)\Omega \tag{11}$$

$$\frac{\Delta H_m}{\Delta H'_m} \approx \frac{(a_{AE} - a_{BE})^2}{(a'_{AE} - a'_{BE})^2} \tag{12}$$

Using $a_{BE} = a_{Co}(ZnSe) = 2.43$ Å, $a'_{BE} = a_{Co}(CdSe) = 2.48$ Å, $a_{BE} = a_{Zn} = 2.45$ Å, and $a'_{BE} = a_{Cd} = 2.63$ Å (Table 1), a value of $[\Delta H_m(Co^{2+}:CdSe)]/[\Delta H'_m(Co^{2+}:ZnSe)] \approx 39$ is estimated. The relatively large difference between $Co^{2+}-Se^{2-}$ and $Cd^{2+}-Se^{2-}$ bond lengths described by Figure 4 thus destabilizes Co^{2+}:CdSe in a way that has no analogue in Co^{2+}:ZnSe, which has better cation size compatibility.

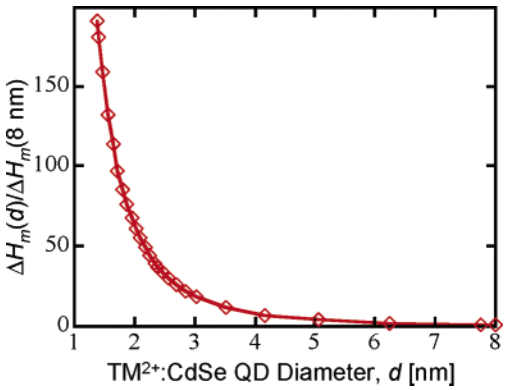

Figure 5. Diameter dependence of excess enthalpy of mixing ($\Delta H_m(d)$) for incorporation of a single TM^{2+} impurity ion into a CdSe nanocrystal of diameter d. Values are normalized to $\Delta H_m(8\ nm)$.

It is important to note that Mn^{2+}-doped CdSe and ZnSe both suffer from equally large bond-length mismatches because $Mn^{2+}-Se^{2-}$ bond lengths happen to fall roughly between a_{Cd} and a_{Zn}. For this comparison, EXAFS studies of 10% Mn^{2+}:CdSe have yielded $a_{Mn}(CdSe) = 2.54$ Å,[6] and those of 15% Mn^{2+}:ZnSe have yielded $a_{Mn}(ZnSe) \approx 2.55$ Å,[8] from which $[\Delta H_m(Mn^{2+}:CdSe)]/[\Delta H'_m(Mn^{2+}:ZnSe)] \approx 1$ is estimated. Clearly, other factors are also important determinants of the relative doping efficiencies of CdSe and ZnSe nanocrystals by Mn^{2+}. This conclusion is consistent with the observation that increased anion concentrations during synthesis will favor Mn^{2+} incorporation into CdSe nanocrystals.[33]

Finally, we note that eq 11 provides a simple explanation for the diameter dependence of nanocrystal doping and, hence, for the driving force for nanocrystal "self-purification."[38] Figure 5 plots the mixing enthalpy $\Delta H_m(d)$ for incorporation of a single TM^{2+} dopant into various CdSe nanocrystals of different diameters, normalized to $\Delta H_m(8\ nm)$. The plot shows a rapidly increasing excess enthalpy of mixing as the nanocrystal diameter decreases and is remarkably similar to that calculated by density functional theory (DFT) methods in ref 38. For example, Figure 5 suggests that the enthalpic cost of doping a $d = 1.4$ nm CdSe nanocrystal is approximately 6.2 times greater than that for doping a $d = 2.6$ nm nanocrystal, compared with the value of 5.8 calculated by DFT. Because a diameter-independent $(a_{AE} - a_{BE})^2$ has been assumed for Figure 5 (an assumption validated by the DFT bond length results[38]), this trend arises ultimately from the corresponding increase in effective dopant concentration as the nanocrystal diameter is reduced. According to eq 11, excess enthalpies of mixing associated with bimodal bond-length distributions such as those shown in Figure 4 therefore clearly favor doping of larger rather than smaller nanocrystals.

4. Conclusion

In summary, the Co^{2+} $^4A_2 \rightarrow {}^4T_1(P)$ ligand-field transition energies of $Cd_{1-x}(Zn + Co)_xSe$ alloy nanocrystals have been found to vary smoothly with the composition parameter, x. Quantitative analysis reveals a bimodal distribution of cation−anion bond lengths in the alloy nanocrystals and hence substantial differences between average and microscopic structures. Such bimodal bond-length distributions cause a diameter-

(32) Malik, M. A.; O'Brien, P.; Revaprasadu, N. *J. Mater. Chem.* **2001**, *11*, 2382−2386.
(33) Erwin, S. C.; Zu, L. J.; Haftel, M. I.; Efros, A. L.; Kennedy, T. A.; Norris, D. J. *Nature* **2005**, *436*, 91−94.
(34) Davis, K. J.; Dove, P. M.; De Yoreo, J. J. *Science* **2000**, *290*, 1134−1137.
(35) Stringfellow, G. B. *J. Cryst. Growth* **1974**, *27*, 21−34.
(36) Martins, J. L.; Zunger, A. *Phys. Rev. B* **1984**, *30*, 6217−6220.
(37) Srivastava, G. P.; Martins, J. L.; Zunger, A. *Phys. Rev. B* **1985**, *31*, 2561−2564.
(38) Dalpian, G. M.; Chelikowsky, J. R. *Phys. Rev. Lett.* **2006**, *96*, 226802.

dependent enthalpic destabilization of doped nanocrystals that undoubtedly contributes to the difficulties sometimes encountered in efforts to dope semiconductor nanocrystals.[17,18,32,33,39]

Acknowledgment. This research was funded by the NSF (PECASE DMR-0239325, DGE-0504573 (IGERT fellowship to S.A.S.), and DMR-0303450 (REU fellowship to E.A.H.)), the Research Corporation, the Dreyfus Foundation, and the Sloan Foundation.

(39) Mikulec, F. V.; Kuno, M.; Bennati, M.; Hall, D. A.; Griffin, R. G.; Bawendi, M. G. *J. Am. Chem. Soc.* **2000**, *122*, 2532−2540.

Note Added after ASAP Publication: Due to a production error, equation 10 incorrectly displayed n times the square root, in the version published March 13, 2007; the correct version, expressing the n-th root, was published on March 14, 2007.

Supporting Information Available: Additional absorption spectra (one figure). This information is available free of charge via the Internet at http://pubs.acs.org.

JA068260P